Tensile strain engineering of germanium micro-disks on free-standing SiO_2 beams

2016 Jpn. J. Appl. Phys. 55 04EH02

(http://iopscience.iop.org/1347-4065/55/4S/04EH02)

Japanese Journal of Applied Physics **55**, 04EH02 (2016)
http://doi.org/10.7567/JJAP.55.04EH02

REGULAR PAPER

Tensile strain engineering of germanium micro-disks on free-standing SiO_2 beams

Abdelrahman Z. Al-Attili[1], Satoshi Kako[2], Muhammad K. Husain[1], Frederic Y. Gardes[1], Satoshi Iwamoto[2], Yasuhiko Arakawa[2], and Shinichi Saito[1]*

[1]*Nanoelectronics and Nanotechnology Research Group, Faculty of Physical Sciences and Engineering, University of Southampton, Southampton SO17 1BJ, U.K.*
[2]*Insititute of Industrial Science, the University of Tokyo, Meguro, Tokyo 153-8505, Japan*

*E-mail: S.Saito@soton.ac.uk

Received September 20, 2015; revised December 5, 2015; accepted December 28, 2015; published online March 2, 2016

Tensile strain is required to enhance light-emitting direct-gap recombinations in germanium (Ge), which is a promising group IV material for realizing a monolithic light source on Si. Ge micro-disks on free-standing SiO_2 beams were fabricated using Ge-on-Insulator wafers for applying tensile strain to Ge in a structure compatible with an optical confinement. We have studied the nature of the strain by Raman spectroscopy in comparison with finite-element computer simulations. We show the impacts of the beam design on the corresponding strain value, orientation, and uniformity, which can be exploited for Ge light emission applications. It was found that the tensile strain values are larger if the length of the beam is smaller. We confirmed that both uniaxial and biaxial strain can be applied to Ge disks, and maximum strain values of 1.1 and 0.6% have been achieved, as confirmed by Raman spectroscopy. From the photoluminescence spectra of Ge micro-disks, we have also found a larger energy-splitting between the light-hole and the heavy-hole bands in shorter beams, indicating the impact of tensile strain.

1. Introduction

Engineering of energy-bands structures and carrier dynamics by lattice deformation is a promising pathway to revolutionize the performance of semiconductor devices.[1–3] For example, strain application has been used to enhance channel mobility in complementary metal–oxide–semiconductor field-effect transistors (CMOSFETs).[2] It was also exploited to expand the detection wavelength of germanium (Ge) photo-detectors.[4,5] Application of tensile strain is expected to play a key role in developing a Ge-based laser diode compatible with CMOS processes.[6–10] Tensile strain is essential to transform Ge into an optical gain material.[3,8,9,11] In fact, lasing of tensile-strained Ge Fabry–Perot (FP) structures was reported by optical[12] and electrical[13,14] pumping. Lasing of GeSn alloys was also reported under optical pumping at low tempeartures.[15]

In order to further reduce the lasing threshold and allow for efficient room-temperature operation, it is necessary to increase the strain values, in addition to introducing high n-type doping.[16] Tensile strain shrinks the total band-gap of Ge, and reduces the energy difference between the direct (Γ) valley and the indirect (L) valley in the conduction band.[3,9,10] Consequently increasing the probability of electrons injection in the Γ valley and enhancing the light-emitting direct-gap recombinations.[9,10] Moreover, besides the value of strain, uniformity of its distribution is crucial for light-emitting purposes.[17–20] Non-uniformity of strain is translated into variations of Ge band-gap, eventually creating optical gain and loss regions within the same Ge structure.[19–23]

Several approaches were proposed to enhance the tensile strain, which is limited to approximately 0.2% after the direct epitaxial growth of Ge layer on Si.[10,24,25] The use of buffer layers, with lattice mismatch relative to Ge, is capable of delivering high and tuneable strain values on relatively thin Ge layers or quantum dots. By using $In_xGa_{1-x}As$ layers, for example, the tensile strain was increased up to 1.37%, depending on the indium content (x).[26] Such an approach might be suitable for quantum-well devices, yet requires the introduction of III–V materials in a CMOS line. Deposition of external stressors such as Si_3N_4 is tempting as a mature CMOS process.[21–23] The use of Si_3N_4 stressors on Ge waveguides,[17,22,23,27,28] and micro-disks,[18–20] is reported for light emission applications. Uniformity of the resulting strain is an issue to be explored,[19,20,22,23] since the strain distribution is highly dependent on the geometry. In the case of Ge micro-disks, uniformity of the strain can be enhanced by fabricating the disks on pillars rather than pedestals,[19] or depositing Si_3N_4 on the top and the bottom sides of the disk.[20] Highest reported tensile strain values were obtained through fabricating free-standing Ge beams.[29–31] Such strain can be manipulated by changing the dimensions of the free-standing beam and the suspension region. Additional stressor layers can be added on the beam sides for enhancing the strain.[30] Uniaxial tensile strain of 3.1%,[29] and 5.7%,[31] were reported. Being uniaxial, this strain has a reduced effect on the band-gap of Ge, where a uniaxial strain of approximately 4.7% is required to convert Ge into a direct-gap material,[29,31] compared to ∼2.0% biaxial tensile strain.[3] Even though extremely high tensile strain values can be achieved by suspension, embedding an optical cavity within such structures is challenging, which is necessary to observe resonant emission.

We previously proposed Ge micro-disks on free-standing silicon-dioxide beams to combine high tensile strain and optical confinement using Ge-on-Insulator (GOI) wafers.[32] By releasing the highly-stressed thermally-grown buried oxide (BOX) layer, we applied tensile strain on Ge micro-disks and observed Whispering–Gallery Modes (WGMs).[18,32–35] However, the exact mechanism and nature of tensile strain applied to the Ge micro-disks have not been completely elucidated, yet.

In this paper, we investigate the mechanism of the tensile strain obtained by fabricating various SiO_2 beam structures with Ge micro-disks on top. Rectangular beams with straight edges and boundaries determined by anisotropic wet etching of Si were designed, in order to restrict the resulting strain to the beam suspension and reduce the effect of the boundaries. A comparison with finite-element simulations is conducted to examine the impact of the beam design on the orientation,

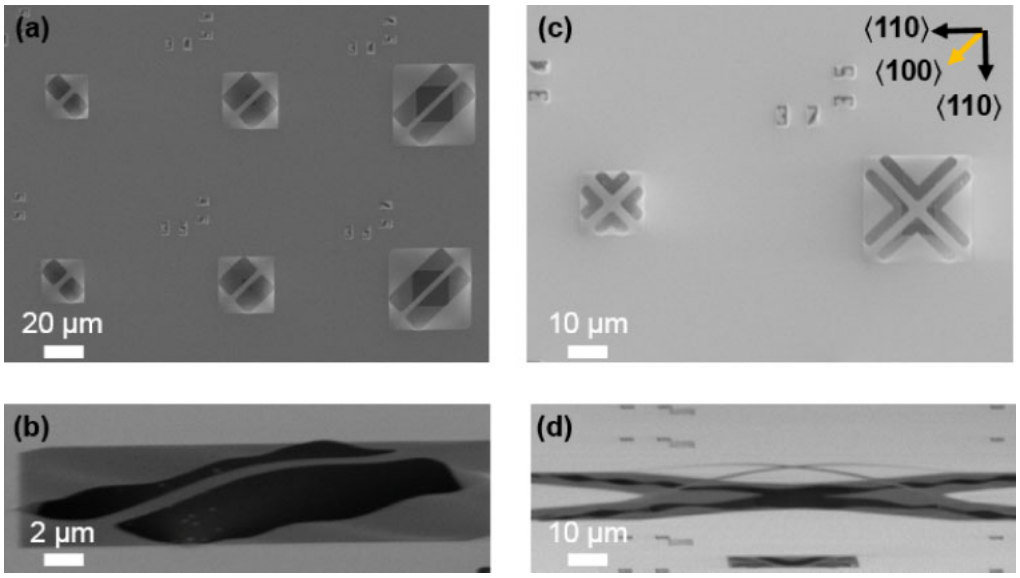

Fig. 1. (Color online) Scanning electron microscopy images of SiO_2 beams: (a) top, and (b) birds-eye view of uniaxial beams. (c) Top, and (d) birds-eye view of biaxial beams. Birds-eye view shows that the beams are significantly deflected upwards as an indication of tensile strain accumulation on top. Beams are aligned along ⟨100⟩ directions.

distribution, and value of the resulting strain. Raman spectroscopy measurements were conducted on Ge micro-disks on free-standing SiO_2 beams with different dimensions, confirming the accumulation of tensile strain, and validating the simulations results of higher tensile strain values for the beams with smaller lengths. Moreover, photoluminescence measurements show that the splitting between the light- and heavy-hole peaks is increased for smaller beam lengths, indicating a higher tensile strain.

2. Experimental methods

To fabricate Ge micro-disks on free-standing SiO_2 beams, we used a commercially available GOI wafer with 100-nm-thick Ge and 145-nm-thick BOX layers, which was manufactured by a layer transfer technology using a Ge layer grown on a virtual substrate, which was bonded onto a silicon substrate with the thermal oxide.[36–39] After cleaning the wafers using hydrofluoric (HF) hydrochloric (HCl) acids, Ge disks were dry etched by reactive-ion etching (RIE). Then, a 100-nm-thick layer of SiO_2 was deposited using plasma-enhanced chemical vapor deposition (PECVD) at 350 °C, to protect the disks from the following processing steps. The beams were made by patterning the BOX layer using a dry etching process down to the thickness of 20 nm, and a subsequent wet etching to avoid any plasma-induced damage to the surface of the bulk Si substrate for the following alkali etching. The structures were then suspended by anisotropic wet-etching using tetra-methyl-ammonium hydroxide (TMAH). Uniaxial and biaxial beams were fabricated as shown in Fig. 1, aligned with the ⟨100⟩ directions. Alignment along the ⟨100⟩ directions is required to result in free-standing structures, due to anisotropy of alkali wet-etching along the ⟨110⟩ directions. Beam lengths (L) were varied from 10 to 100 μm, while beam widths (W) were varied from 1 to 12 μm.

After suspension, most of the beams deflected due to the relief of residual stresses within the thermally-grown oxide, as expected.[40,41] Residual stresses are inherent within the thermally-grown SiO_2 due to high growth temperatures and the difference in thermal expansion coefficients between SiO_2 and Si.[40] As a result of beam deflection, strain is distributed across the structure, imposing tensile strain on the top surface of the upward deflected beams.[41] As shown in Fig. 1, uniaxial and biaxial SiO_2 beams [Figs. 1(a) and 1(c)] were significantly deflected upwards [Figs. 1(b) and 1(d)], indicating the accumulation of tensile strain on the top surface. This strain will be applied to a Ge disk on the beam, such that the strain value and orientation can be manipulated through the beam design.

3. Results and discussion

3.1 Computer simulations

Three-dimensional computer simulations were performed in order to examine the effect of the beam design on the value, orientation, and distribution of the resulting strain due to suspended SiO_2 beams. We mapped the simulation results of a 20-μm-long uniaxial beam with 2 μm Ge disk on top, to the experimental data found by Raman spectroscopy of a similar structure. Such that the experimental strain value measured at the top of the Ge disk was set to match the simulated strain value at the top center point of the Ge disk. This matching was done by assuming a uniform force affecting the bottom side of the beam to account for the residual stresses,[41] and the value of this force was fit to approximately 700 μN. The model was then used to investigate other structures including beams with different dimensions, and biaxial beams. We have also assumed that the beams deflect upwards into the first eigenmode with fixed boundary conditions. This assumption is sufficient to investigate the distribution of strain within the structure, and the dependency on the design parameters such as the beam length (L).

Initially, we simulated uniaxial and biaxial beams with similar dimensions. Thicknesses of Ge and BOX layers were set to 100 and 145 nm, respectively, to match the fabricated devices. While the beam length (L) was set to 20 μm and the beam width (W) was 4 μm. Strain components ϵ_x, ϵ_y, and ϵ_z are defined as the relative change in displacement along

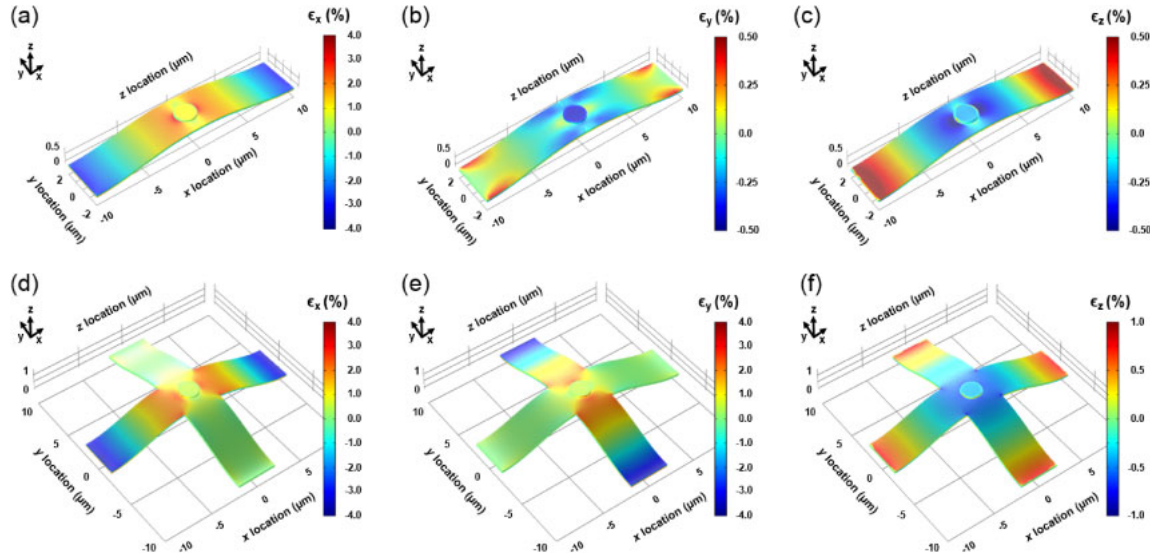

Fig. 2. (Color online) Three-dimensional simulations showing the distribution of normal strain components: (a) ϵ_x, (b) ϵ_y, and (c) ϵ_z, across a uniaxial SiO_2 beam with a 2 μm Ge disk on top. While (d), (e), and (f), show the same components' distribution for a biaxial beam with similar dimensions. The length of the beams is 20 μm and the width is 4 μm.

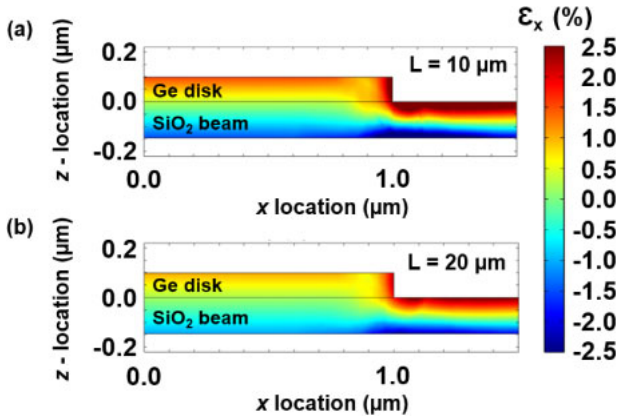

Fig. 3. (Color online) Cross-sectional map of the strain component along the beam direction (ϵ_x) within a 2 μm Ge disks on a: (a) 10 μm, and (b) 20 μm long uniaxial SiO_2 beam.

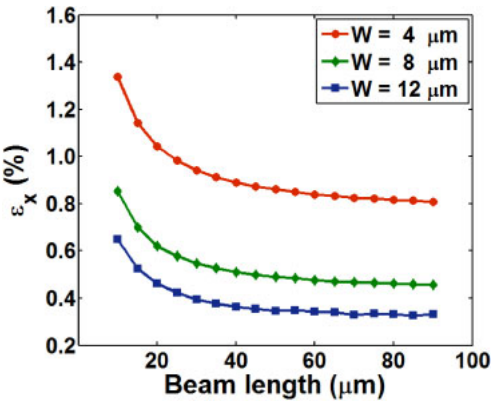

Fig. 4. (Color online) Simulated strain component along the beam direction (ϵ_x) for uniaxial SiO_2 beams with different lengths varying from 10 to 90 μm, and widths of 4, 8, and 12 μm.

the three principal axes x, y, and z, and typical strain distributions for a uniaxial beam and a biaxial beam are shown in Figs. 2(a)–2(c) and Figs. 2(d)–2(f), respectively. In the uniaxial beam, only one tensile strain component (ϵ_x) along the beam direction (x) dominates over one order of magnitude weaker compressive strains along the other in-plane (ϵ_y) and the out-of-plane (ϵ_z) directions. On the other hand, in biaxial beams, the two in-plane components (ϵ_x and ϵ_y) are identical reflecting the symmetry and the tensile nature, while the out-of-plane (ϵ_z) component is compressive. The maximum value of the strain component ϵ_x was larger in the uniaxial beam, compared with the strain components ϵ_x and ϵ_y in the biaxial beam. However, the total tensile change in volume is higher in the biaxial beams. Accordingly, biaxial beams would impose more significant impacts on deforming the band structures of Ge.

Figure 3 shows the cross-sectional distribution of strain component along the beam direction (ϵ_x), for uniaxial beams with different lengths of 10 μm [Fig. 3(a)] and 20 μm [Fig. 3(b)]. It was found that tensile strain is accumulated throughout most of the disk. In addition, we found that shorter beams have slightly higher tensile strain, although the strain is more non-uniformly distributed. The non-uniformity of strain would result in the local variations of the band-gap of Ge,[18–20] so that highly-strained regions have lower Γ valleys,[1,3] increasing the population of electrons within these regions compared to less tensile-strained regions. Remarkably, as shown in Fig. 3, the highly-strained regions are expected at the edge of the disk, which is favorable for whispering gallery modes (WGM). In our simulations, we assumed fixed boundary conditions at the edges of the beam. However, it is difficult to accurately estimate the boundary conditions for a real device, depending on either being rigidly fixed, or easily deformed. The strain distribution within the disk would also depend on the adhesion between Ge and BOX layers, where the poor adhesion would cause a loss of strain at the interface due to the relaxation of the Ge layer.

Figure 4 shows a representation of the strain dependence on the beam length (L) and the width (W) of uniaxial SiO_2

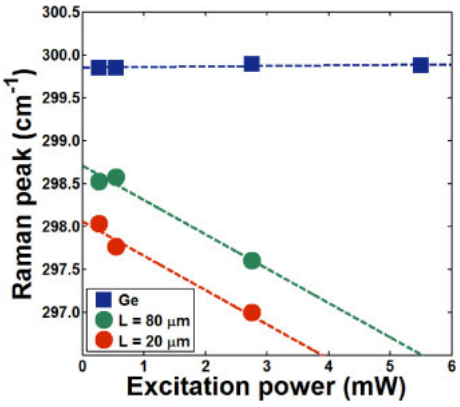

Fig. 5. (Color online) Power dependence of Raman peak position for bulk Ge, and 2 μm Ge disks on free-standing SiO_2 beams with different lengths. Dashed lines are best fit linear relations. In free-standing structures, a significant linear redshift is observed in the Raman peak position with higher excitation power.

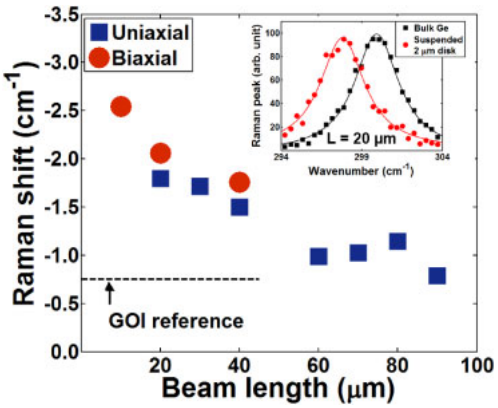

Fig. 6. (Color online) Experimental Raman shift values for 2 μm Ge disks on uniaxial and biaxial free-standing SiO_2 beams with different lengths. Inset shows Raman spectra for bulk Ge, and a Ge micro-disk on 20-μm-long uniaxial SiO_2 beam. Higher strain values are observed in shorter beams.

beams. The strain component along the beam direction (ϵ_x) is measured at the center top point of the Ge disk. Shorter beams are found to have higher tensile strain values, and this effect is pronounced for beams shorter than 20 μm. On the other hand, the strain is reduced for longer beams until it saturates to a certain value, and the dependence on L becomes negligible. The beam width (W) has a similar effect on ϵ_x, yet having a slightly less impact compared with L. Accordingly, for a certain stack of Ge and BOX, there is a maximum achievable tensile strain determined by the minimum beam dimensions. It is possible to further increase the strain by changing the stack ratio. For instance, using a thinner Ge layer permits the application of higher strain on the entire disk. Increasing the thickness of the BOX layer is expected to have a similar effect due to the higher strain accumulated on the beam.

3.2 Strain characterization

Raman spectroscopy measurements were conducted to confirm the accumulation of tensile strain within the structures, and the validity of simulation results. The shifts in Raman peak relative to bulk Ge ($\Delta\omega$) were related to strain (ϵ) by a proportionality factor, where $\Delta\omega = C \times \epsilon$. This proportionality factor, C, was reported to be 152 cm^{-1} for ⟨100⟩ uniaxial strain,[29,31] and 390 cm^{-1} for biaxial strain.[22,23] A laser with 532 nm wavelength was used to excite the Ge disks, and the Raman signal was collected through an objective lens with a magnification of 50 and analyzed with a 3000 line/mm grating to determine the peak position. Due to heating effects on suspended structures by laser excitation, we measured the shifts of Raman peak positions by increasing the laser power at the surface of the sample from 275 to 2750 μW. It was found that heating induces an additional redshift in the Raman peak position, linearly proportional to excitation power. Then we extrapolated the measured points in order to estimate the Raman peak position without the heating effect at the limit of negligible excitation power. For instance, a power-induced Raman shift of 0.6×10^{-5} and -5.12×10^{-5} cm^{-1}/μW were observed for bulk Ge and non-patterned GOI wafers, respectively. While a power-induced shift of -38.04×10^{-5} and -39.93×10^{-5} cm^{-1}/μW, were observed for Ge micro-disks on free-standing SiO_2 beams with a length of 20 and 80 μm, respectively, as shown in Fig. 5. We found more than 60-times increase in the sensitivity of Raman peak position to excitation power in free-standing structures compared to bulk Ge, presumably due to the absence of the heat leakage path through the bulk substrate, which is replaced by air.

Figure 6 shows the measured Raman shift values for uniaxial and biaxial beams with different lengths and a fixed width of 4 μm. The inset shows the actual Raman spectra for bulk Ge, and a Ge micro-disk on free-standing SiO_2 beam ($L = 20$ μm). Accumulation of tensile strain within the Ge disks after suspension was found according to the negative Raman shift value compared with the reference of the non-suspended GOI wafer. It was also found that shorter beams resulted in higher negative Raman shifts, and thus higher tensile strain, for both uniaxial and biaxial beams. For example, Raman shifts of −1.79, −1.5, −0.98, and −0.78 cm^{-1} were measured for uniaxial beams with lengths of 20, 40, 60, and 90 μm, respectively. These correspond to a uniaxial tensile strain of 1.17, 0.98, 0.64, and 0.51%, respectively. Moreover, biaxial beams had slightly higher negative Raman shifts compared to uniaxial beams with similar dimensions. Raman shifts of −2.5, −2, and −1.7 cm^{-1} were measured for biaxial beams with lengths of 10, 20, and 40 μm, respectively. These correspond to a biaxial tensile strain of 0.6, 0.5, and 0.4%, respectively. These experimental results agree with the simulations presented in the previous section, and imply that for light emission purposes, higher strain values are required.

We have also conducted a photoluminescence (PL) study at room temperature on Ge micro-disks on free-standing uniaxial SiO_2 beams. A CW laser source with a wavelength of 730 nm was used to pump the Ge disks from top through an objective lens with a magnification of 50 times. Figure 7 shows the power dependence of the PL spectra for a Ge micro-disk on 10-μm-long uniaxial beam. The PL signal around 1580 nm corresponds to the direct-gap emission of Ge.[6–10,16,32] As the pumping power is increased from 100 to 1000 μW, it is found that the position of the shorter-wavelength peak, which corresponds to Γ-heavy hole (HH) recombinations,[1,3,8,10] remains nearly fixed. This indicates that the temperature within the disk has not increased

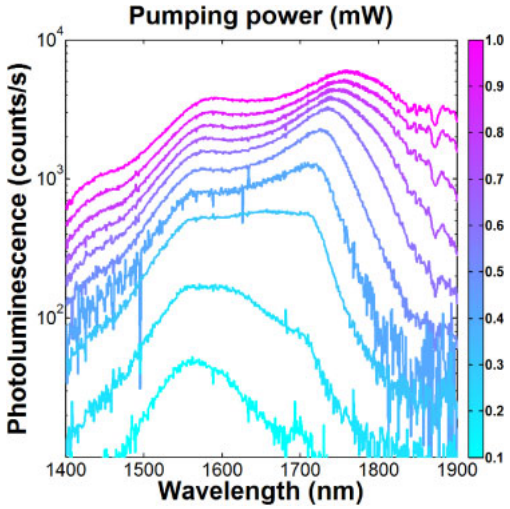

Fig. 7. (Color online) Photoluminescence spectra of a Ge micro-disk on 10-μm-long uniaxial SiO_2 beam using different pumping powers. The spectra consist of two distinctive peaks, which are attributed to Γ-HH (lower wavelength) and Γ-LH (higher wavelength) recombinations. As the power increases, the Γ-HH peak remains nearly fixed while the Γ-LH peak is significantly red-shifted, presumably due to an additional strain induced by the deformation of the beam due to heating upon laser excitation.

significantly. Meanwhile, the higher-wavelength peak, which is mainly attributed to Γ-light hole (LH) recombinations,[1,3,8,10] is remarkably red-shifted. This might originate from the deformation of the beam due to heating by laser excitation, imposing an additional strain which induces the separation of LH and HH bands,[1,3,8] and consequently broadening the spectrum. We did not observe any sharp-peak resonances from cavity modes in 2 μm disks. The exact origin of the absence of peaks has not been clarified, yet, but the quality factors of cavities would be small due to the small radius. The surface-carrier recombination effect would also be pronounced for dry-etched GOI structures, which may affect the lifetime of the carriers. A proper chemical treatment of the surface and a suitable passivation layer can be used to terminate the dangling bonds at the surface and enhance carriers' lifetime.[6,42]

PL spectra for 2 μm Ge disks on uniaxial SiO_2 beams with different lengths, varying from 10 to 90 μm, are shown in Fig. 8. As the pumping power was set to 400 μW with a spot-size of ∼2 μm, and the size of the disk is fixed, the heating effects are expected to be similar regardless of the beam length. It was found that as the beam length decreases, the PL spectrum gets broadened, with two distinctive peaks as shown in Fig. 8(a). The shorter and longer-wavelength peaks are attributed to Γ-HH and Γ-LH recombinations,[1,3,8,10] respectively. By fitting these peaks with Lorentzian functions, we estimated the peak positions for all beam lengths. The positions for Γ-HH and Γ-LH peaks are plotted in Fig. 8(b) with the best-fit line for each dataset. The separation between these two peaks increases as the beam length decreases. For instance, a separation of approximately 87 nm is observed for a 70-μm-long beam, while a separation of 139 nm is observed for a 10-μm-long beam. This can be explained by the accumulation of additional tensile strain within the Ge disks for shorter beams, inducing a separation in HH and LH bands.[1,3,8]

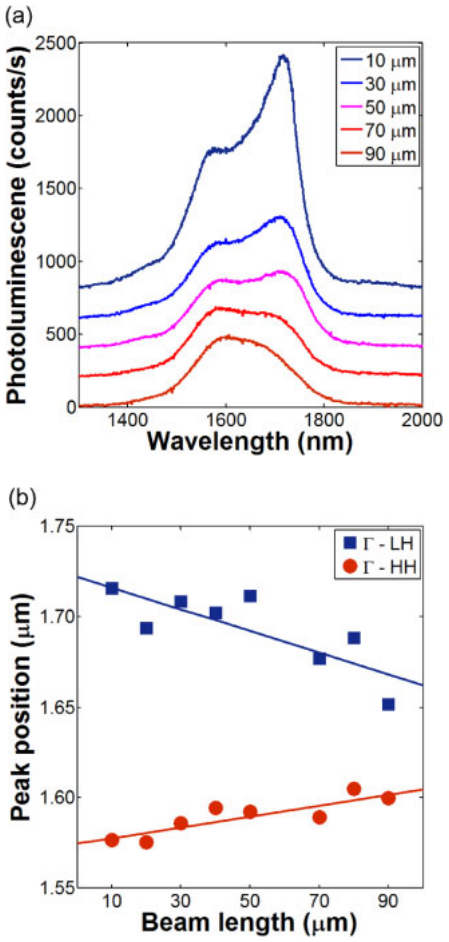

Fig. 8. (Color online) (a) Photoluminescence spectra of Ge micro-disks on free-standing uniaxial SiO_2 beams with different lengths. The spectra consist of two distinctive peaks which are attributed to Γ-HH (lower wavelength) and Γ-LH (higher wavelength) recombinations. (b) Corresponding Γ-HH and Γ-LH peak positions for beams with different lengths. As the beam length decreases, the energy-splitting between Γ-HH and Γ-LH peaks increases, indicating an enhancement in tensile strain.

4. Conclusions

We have investigated the strain accumulated within Ge micro-disks on free-standing SiO_2 beams, using computer simulations and Raman spectroscopy. It was found that the strain orientation, distribution, and value is affected by the beam design. Uniaxial and biaxial beams were shown to apply a different type of strain, consequently having a different effect on the bandgap of Ge. Strain distribution within the disks shows that tensile strain is predominant, yet with slight variations especially at the edges. Additionally, shorter beams were expected to impose higher tensile strain values, and this was confirmed by Raman spectroscopy. PL measurements also show that the strain is enhanced in shorter beams, represented by a larger splitting between the Γ-HH and Γ-LH peaks. Although a maximum uniaxial strain of approximately 1.1% was measured by Raman, we expect that the poor adhesion between the Ge and BOX layers results in a strain loss at the interface. Enhancement of strain requires the fabrication of shorter beams, engineering the Ge/BOX stack thicknesses, and improving the adhesion between the Ge and BOX layers. We believe that the use of thermally-grown BOX layer as a stressor is advantageous to investigate the optical characteristics of Ge with excellent crystalline quality.

Acknowledgments

We would like to thank research collaborators, engineers, and line managers in Hitachi, the University of Tokyo, and University of Southampton for supporting this project. We would also like to thank the technical support team of COMSOL Multiphysics simulations software, especially Dr. Robbie Balcombe. Parts of the studies discussed here was supported by Japan Society for the Promotion of Science (JSPS) through its "Funding Program for World-Leading Innovation R&D on Science and Technology (FIRST Program)", the Project for Developing Innovation Systems, and Kakenhi 216860312, MEXT, Japan. This work is also supported by EU, FP7, Marie-Curie, Carrier Integration Grant (CIG), PCIG13-GA-2013-618116, EPSRC standard grant (EP/M009416/1), EPSRC manufacturing fellowship (EP/M008975/1), and University of Southampton, Zepler Institute, Research Collaboration Stimulus Fund. The data in this paper can be obtained from the University of Southampton ePrints research repository: http://dx.doi.org/10.5258/SOTON/386418.

1) C. G. Van de Walle, Phys. Rev. B **39**, 1871 (1989).
2) M. V. Fischetti and S. E. Laux, J. Appl. Phys. **80**, 2234 (1996).
3) M. El Kurdi, G. Fishman, S. Sauvage, and P. Boucaud, J. Appl. Phys. **107**, 013710 (2010).
4) Y. Ishikawa, K. Wada, J. Liu, D. D. Cannon, H.-C. Luan, J. Michel, and L. C. Kimerling, J. Appl. Phys. **98**, 013501 (2005).
5) X. Wang, H. Li, R. Camacho-Aguilera, Y. Cai, L. C. Kimerling, J. Michel, and J. Liu, Opt. Lett. **38**, 652 (2013).
6) S. Saito, F. Y. Gardes, A. Z. Al-Attili, K. Tani, K. Oda, Y. Suwa, T. Ido, Y. Ishikawa, S. Kako, S. Iwamoto, and Y. Arakawa, Front. Mater. **1**, 15 (2014).
7) S. Saito, K. Oda, T. Takahama, K. Tani, and T. Mine, Appl. Phys. Lett. **99**, 241105 (2011).
8) X. Sun, J. Liu, L. C. Kimerling, and J. Michel, IEEE J. Sel. Top. Quantum Electron. **16**, 124 (2009).
9) J. Liu, R. Camacho-Aguilera, J. T. Bessette, X. Sun, X. Wang, Y. Cai, L. C. Kimerling, and J. Michel, Thin Solid Films **520**, 3354 (2012).
10) J. Liu, L. C. Kimerling, and J. Michel, Semicond. Sci. Technol. **27**, 094006 (2012).
11) J. Liu, X. Sun, L. C. Kimerling, and J. Michel, Opt. Lett. **34**, 1738 (2009).
12) J. Liu, X. Sun, R. Camacho-Aguilera, L. C. Kimerling, and J. Michel, Opt. Lett. **35**, 679 (2010).
13) R. Koerner, M. Oehme, M. Gollhofer, M. Schmid, K. Kostecki, S. Bechler, D. Widmann, E. Kasper, and J. Schulze, Opt. Express **23**, 14815 (2015).
14) R. E. Camacho-Aguilera, Y. Cai, N. Patel, J. T. Bessette, M. Romagnoli, L. C. Kimerling, and J. Michel, Opt. Express **20**, 11316 (2012).
15) S. Wirths, R. Geiger, N. von den Driesch, G. Mussler, T. Stoica, S. Mantl, Z. Ikonic, M. Luysberg, S. Chiussi, J. M. Hartmann, H. Sigg, J. Faist, D. Buca, and D. Grützmacher, Nat. Photonics **9**, 88 (2015).
16) A. Z. Al-Attili, S. Kako, M. K. Husain, F. Y. Gardes, H. Arimoto, N. Higashitarumizu, S. Iwamoto, Y. Arakawa, Y. Ishikawa, and S. Saito, Jpn. J. Appl. Phys. **54**, 052101 (2015).
17) A. Ghrib, M. de Kersauson, M. El Kurdi, R. Jakomin, G. Beaudoin, S. Sauvage, G. Fishman, G. Ndong, M. Chaigneau, R. Ossikovski, I. Sagnes, and P. Boucaud, Appl. Phys. Lett. **100**, 201104 (2012).
18) A. Ghrib, M. El Kurdi, M. de Kersauson, M. Prost, S. Sauvage, X. Checoury, G. Beaudoin, I. Sagnes, and P. Boucaud, Appl. Phys. Lett. **102**, 221112 (2013).
19) A. Ghrib, M. El Kurdi, M. Prost, M. de Kersauson, L. Largeau, O. Mauguin, G. Beaudoin, S. Sauvage, X. Checoury, G. Ndong, M. Chaigneau, R. Ossikovski, S. David, I. Sagnes, and P. Boucaud, Proc. SPIE **8990**, 89901C (2014).
20) A. Ghrib, M. El Kurdi, M. Prost, S. Sauvage, X. Checoury, G. Beaudoin, M. Chaigneau, R. Ossikovski, I. Sagnes, and P. Boucaud, Adv. Opt. Mater. **3**, 353 (2015).
21) C. Ortolland, Y. Okuno, P. Verheyen, C. Kerner, C. Stapelmann, M. Aoulaiche, N. Horiguchi, and T. Hoffmann, IEEE Trans. Electron Devices **56**, 1690 (2009).
22) G. Capellini, G. Kozlowski, Y. Yamamoto, M. Lisker, C. Wenger, G. Niu, P. Zaumseil, B. Tillack, A. Ghrib, M. de Kersauson, M. El Kurdi, P. Boucaud, and T. Schroeder, J. Appl. Phys. **113**, 013513 (2013).
23) G. Capellini, C. Reich, S. Guha, Y. Yamamoto, M. Lisker, M. Virgilio, A. Ghrib, M. El Kurdi, P. Boucaud, B. Tillack, and T. Schroeder, Opt. Express **22**, 399 (2014).
24) Y. Ishikawa, K. Wada, D. D. Cannon, J. Liu, H.-C. Luan, and L. C. Kimerling, Appl. Phys. Lett. **82**, 2044 (2003).
25) J. Liu, X. Sun, D. Pan, X. Wang, L. C. Kimerling, T. L. Koch, and J. Michel, Opt. Express **15**, 11272 (2007).
26) Y. Bai, K. E. Lee, C. Cheng, M. L. Lee, and E. A. Fitzgerald, J. Appl. Phys. **104**, 084518 (2008).
27) K. Tani, K. Oda, J.-I. Kasai, T. Okumura, T. Mine, S.-I. Saito, and T. Ido, IEEE 10th Int. Conf. Group IV Photonics (GFP), 2013, p. 134.
28) K. Tani, K. Oda, T. Okumura, T. Takezaki, J. Kasai, T. Mine, and T. Ido, Int. Conf. Solid State Devices and Materials (SSDM), 2013, p. 1032.
29) M. J. Süess, R. Geiger, R. A. Minamisawa, G. Schiefler, J. Frigerio, D. Chrastina, G. Isella, R. Spolenak, J. Faist, and H. Sigg, Nat. Photonics **7**, 466 (2013).
30) J. R. Jain, A. Hryciw, T. M. Baer, D. A. B. Miller, M. L. Brongersma, and R. T. Howe, Nat. Photonics **6**, 398 (2012).
31) D. S. Sukhdeo, D. Nam, J.-H. Kang, M. L. Brongersma, and K. C. Saraswat, Photonics Res. **2**, A8 (2014).
32) A. Z. Al-Attili, S. Kako, M. K. Husain, F. Y. Gardes, N. Higashitarumizu, S. Iwamoto, Y. Arakawa, Y. Ishikawa, H. Arimoto, K. Oda, T. Ido, and S. Saito, Front. Mater. **2**, 43 (2015).
33) P. H. Lim, Y. Kobayashi, S. Takita, Y. Ishikawa, and K. Wada, Appl. Phys. Lett. **93**, 041103 (2008).
34) G. Shambat, S.-L. Cheng, J. Lu, Y. Nishi, and J. Vuckovic, Appl. Phys. Lett. **97**, 241102 (2010).
35) S.-L. Cheng, G. Shambat, J. Lu, H.-Y. Yu, K. Saraswat, T. I. Kamins, J. Vuckovic, and Y. Nishi, Appl. Phys. Lett. **98**, 211101 (2011).
36) M. Bruel, Electron. Lett. **31**, 1201 (1995).
37) D. S. Yu, A. Chin, C. C. Liao, C. F. Lee, C. F. Cheng, M. F. Li, W. J. Yoo, and S. P. McAlister, IEEE Electron Device Lett. **26**, 118 (2005).
38) L. Chen, P. Dong, and M. Lipson, Opt. Express **16**, 11513 (2008).
39) M. El Kurdi, T. Kociniewski, T.-P. Ngo, J. Boulmer, D. Débarre, P. Boucaud, J. F. Damlencourt, O. Kermarrec, and D. Bensahel, Appl. Phys. Lett. **94**, 191107 (2009).
40) C. W. Wilmsen, E. G. Thompson, and G. H. Meissner, IEEE Trans. Electron Devices **19**, 122 (1972).
41) S. D. Senturia, *Microsystem Design* (Kluwer, Boston, MA, 2001).
42) J. R. Haynes and W. Shockley, Phys. Rev. **81**, 835 (1951).